EAI Endorsed Transactions
on Energy Web
Research Article EAI.EU

Topology optimization and collaborative development planning of electro-hydrogen coupling based on multi-objective solution algorithms

Xiaowei Li[1,*], Guoxian Luo[2], Dandan Li[1] and Peng Yan[3]

[1]Guangxi Power Grid Co., Ltd., Nanning 530012, China
[2]Baise Power Supply Bureau, Baise 533000, China
[3]China Energy Engineering Group Guangdong Electric Power Design Institute Co., Ltd., Guangzhou 510663, China

Abstract

INTRODUCTION: Renewable energy microgrids need planning methods to manage volatility and balance performance.
OBJECTIVES: Develop a collaborative planning method for electro-hydrogen coupling systems, optimizing economy, environment and reliability.
METHODS: Build a unified planning model for siting, capacity and topology. Solve using improved NSGA-II with adaptive operators and constraint handling.
RESULTS: Based on 8760-hour data, the system increased energy self-sufficiency from 52% to >95%. With 28% extra investment, carbon emissions fell 54% and reliability rose 55%. Lower electrolyzer cost further cut emissions; carbon price at 300 CNY/ton improved scheme competitiveness.
CONCLUSION: Electro-hydrogen coupling enhances microgrid performance. Multi-objective optimization finds the best trade-off. Falling costs and carbon policies will promote system application, aiding low-carbon transformation.

Keywords: electro-hydrogen coupling, microgrid, multi-objective optimization, topological planning, NSGA-II, consumption of renewable energy

Received on 01 November 2025, accepted on 14 December 2025, published on 31 March 2026

doi: 10.4108/ew.12030

1. Introduction

Energy serves as the fundamental guarantee for various activities in modern society, and the stability of the power system supply is closely linked to all industries. With the upgrading of energy consumption structure and digital transformation, the scale of renewable energy power generation, represented by wind and solar energy, is expanding rapidly [1]. Distributed renewable energy, characterized by cleanliness and flexibility, exhibits remarkable advantages in optimizing the energy supply structure and alleviating energy shortages. However, such clean energy generally has inherent volatility and intermittency. Direct integration into the power grid poses challenges to the system's power supply reliability and economic operation [2]. Thus, achieving coordinated interaction between distributed energy and the power grid while ensuring system reliability and further improving economic efficiency remains a complex problem.

Microgrid has garnered widespread attention as an effective integrated solution. It can flexibly interconnect with the main grid via a point of common coupling (PCC), enhancing the autonomy and resilience of regional energy supply [3]. It also supports both islanded operation and grid-

*Corresponding author. Email: LI_XIAO_WEI___@outlook.com

connected modes. Currently, load types integrated into the power grid are becoming increasingly diverse, and the penetration rate of distributed generation is continuously rising. This renders single alternating current (AC) or direct current (DC) microgrid architectures insufficient to fully meet the system's economic and operational efficiency requirements. Therefore, alternating current/direct current (AC/DC) hybrid microgrids have gradually emerged as a more promising development direction [4].

Although microgrid enhances system regulation capabilities, the high proportion of renewable energy integration within it places higher demands on medium and long-term energy balance. Traditional battery energy storage struggles to fully address both emergency backup and large-scale energy storage needs. Against this backdrop, hydrogen, as a green secondary energy source, demonstrates unique value [5]. Through water electrolysis technology, surplus electrical energy from renewable sources can be converted into hydrogen for storage during periods of high generation. During peak electricity demand or insufficient renewable energy output, hydrogen can be converted back to electricity via fuel cells to alleviate peak load pressure. This coupling mechanism of mutual conversion between electricity and hydrogen provides microgrid systems with energy regulation capabilities across different time periods and seasons.

However, constructing an electro-hydrogen coupling system is not straightforward. It constitutes a complex systems engineering project, and its top-level planning is particularly critical [6]. The system involves the capacity configuration and location scheduling of diverse equipment such as wind turbines, photovoltaic panels, electrolyzers, hydrogen storage tanks, and fuel cells; it also comprehensively considers the grid construction timeline throughout the full life cycle. Such systems have high requirements for economic costs during planning and necessitate a balance between multiple objectives, including carbon emissions and power supply reliability [7]. Traditional single-objective optimization methods are no longer sufficient to address such multi-dimensional decision-making needs.

To this end, this study attempts to establish an optimization model integrating topological structure and dynamic development for the multi-objective collaborative planning of microgrid electro-hydrogen coupling systems. After model establishment, an efficient multi-objective solution algorithm is employed to systematically explore the set of Pareto optimal solutions. Its goal is to find a "cost-effective" compromise scheme that maximizes the achievement of these objectives. To verify the proposed method's feasibility and effectiveness, this study conducts simulation analysis based on actual microgrid data from a coastal industrial park. The purpose is to rationally plan distributed energy sources to enhance the economic efficiency of the microgrid system while meeting user needs. Ultimately, it serves as an academic reference and a practical foundation for designing and implementing microgrids in real-world scenarios.

2. Literature review

Optimal planning of microgrids is crucial for ensuring their economical and reliable operation. Early studies focused primarily on the coordinated configuration of "source-storage-load" with batteries as the core component. For instance, Shi et al. [8] constructed a capacity optimization model for wind-solar-storage systems that minimized the total cost of islanded microgrids. Their research verified the effectiveness of batteries in mitigating intraday fluctuations. To further improve power supply quality, Balu et al. [9] introduced reliability constraints into their model, revealing the trade-off between cost and reliability objectives. Similarly, Alsalloum et al. [10] considered the time-of-use (TOU) electricity pricing mechanism. They optimized the interaction strategy between microgrids and the main grid while enhancing system economics. These studies laid the foundation for microgrid planning, but their energy storage systems were mainly designed for short-term regulation. They still had limitations in addressing cross-seasonal energy storage and long-term reliability issues.

To overcome the duration constraints of battery energy storage, hydrogen is introduced into microgrid systems, forming the research direction of electro-hydrogen coupling. Temiz & Dincer [11] designed a wind-solar-hydrogen hybrid system for an isolated community. Simulations showed that hydrogen energy storage significantly improved the system's long-term energy self-sufficiency rate. Moritz et al. [12] took the research a step further. They not only used hydrogen for power generation but also sold surplus hydrogen as a commodity, effectively increasing the investment return of the entire project. In recent years, scholars have begun to focus on optimizing the operation strategies of electro-hydrogen coupling systems. For example, Quan et al. [13] coordinated the operating points of electrolyzers and fuel cells in real time through model predictive control, further tapping the system's regulatory potential. These studies confirmed the technical feasibility of electro-hydrogen coupling and its comprehensive value in improving system economics and resilience from various perspectives.

At the level of planning methods, multi-objective optimization (MOO) algorithms are effective approaches for addressing such problems with conflicting objectives. Among them, advanced evolutionary algorithms like the Non-dominated Sorting Genetic Algorithm II (NSGA-II) have been extensively applied in microgrid capacity configuration research due to their advantages in solving high-dimensional and nonlinear problems. For instance, Teo et al. [14] used NSGA-II to optimize the power source and energy storage capacity of standalone microgrids, clearly revealing the trade-off between cost and reliability. Su et al. [15] applied it to regional integrated energy systems, synchronously optimizing economic and carbon emission objectives. These works verified the applicability of multi-objective algorithms in energy planning.

Nevertheless, a closer examination reveals that most existing applications focus on system capacity configuration decisions—addressing the question of "how large to build". In contrast, the topological connections between equipment (i.e., "how to build and connect") are treated as preconditions or simplified. For geographically distributed microgrids,

equipment siting and network structure also profoundly impact system costs and efficiency. Additionally, most existing electro-hydrogen coupling planning focuses on static ultimate planning, where all equipment is constructed in one go in the initial year of planning. This fails to fully consider the dynamic development characteristics of declining technical costs year by year, creating a gap with the practical engineering demand for phased investment. Hence, building on existing research, this study intends to combine topological optimization with multi-stage collaborative development planning. It constructs a more refined and engineering-oriented multi-objective planning model for electro-hydrogen coupling microgrids. By systematically analyzing the interactive impacts between equipment siting, network layout, and dynamic investment, feasible schemes for the precise planning of microgrids are provided.

3. Research methodology

3.1. Architecture of alternating AC/DC electro-hydrogen coupling microgrid system

The proposed electro-hydrogen coupling microgrid system's topological structure is indicated in Figure 1. This system adopts a hybrid AC/DC bus architecture. Due to the intermittent nature of wind and light output, a combination of the two is adopted on the power supply side. Among the system components, photovoltaic arrays and wind turbines are connected to the DC bus via DC/DC converters. This design minimizes energy conversion links and improves the utilization efficiency of renewable energy. DC loads in the system, such as data centers and electric vehicle charging piles, are directly connected to the DC bus. AC loads, like conventional industrial equipment and air conditioning systems, are linked to the AC bus via inverters. This partitioned power supply method meets the power demand of different loads while avoiding energy losses caused by unnecessary AC/DC conversions.

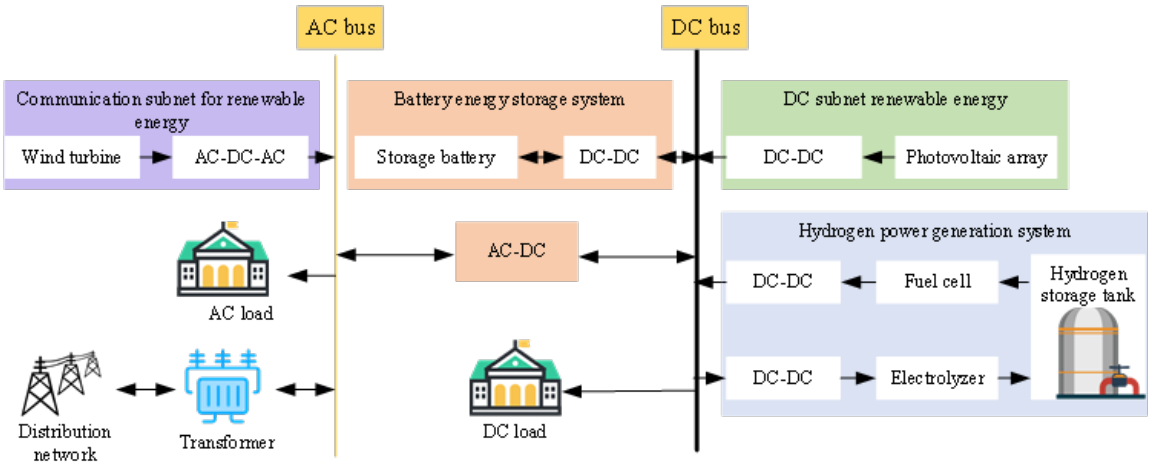

Figure 1. Topological structure of the electro-hydrogen coupling microgrid system

Considering the volatile characteristics of renewable energy output, this study adopts a hybrid energy storage architecture consisting of batteries and a hydrogen energy system. Lithium-ion battery packs are directly connected to the DC bus, responsible for second-to-hour-level power smoothing and frequency regulation. The hydrogen energy system, composed of electrolyzers, hydrogen storage tanks, and fuel cells, undertakes seasonal and cross-day-night energy transfer tasks. When the power generation from renewable energy exceeds the load demand, and the battery is close to full charge, the electrolytic cell starts to operate. This operation converts the excess electrical energy into hydrogen and stores it in hydrogen storage tanks. When renewable energy generation is insufficient, and the battery capacity drops to a set threshold, the fuel cell is activated to convert stored hydrogen into electrical energy. This energy is then input into the power grid, thereby establishing an "electricity-hydrogen-electricity" energy cycle system.

The system maintains flexible interconnection with the upper-level distribution network at the PCC through bidirectional converters. In grid-connected mode, this system can exchange electrical energy with the grid based on electricity price signals and operational needs to achieve more economic operation. In islanded mode, it relies on internal power sources and energy storage systems for an independent power supply, ensuring the continuous capacity for critical loads. It supports the two modes. This flexible interconnection design markedly enhances the system's power supply reliability and operational flexibility.

The system is also equipped with an intelligent energy management system. By real-time monitoring of renewable energy output, load demand, and energy storage status, it

optimizes power distribution according to preset operational strategies to achieve safe, economic, and efficient system operation. The coordinated cooperation between various subsystems enables the system to fully utilize renewable energy while ensuring the reliability and stability of the power supply, offering a complete solution for the park's energy supply.

3.2. The system mathematical model

To quantitatively analyze system operational characteristics, mathematical models for key components need to be established. These models describe the processes of energy generation, conversion, storage, and flow within the system.

(1) Wind-solar power generation models

The photovoltaic array is the photovoltaic power generation system's core component. Its output characteristics are susceptible to external environmental conditions, so an accurate equivalent circuit model is required for analysis, as presented in Figure 2.

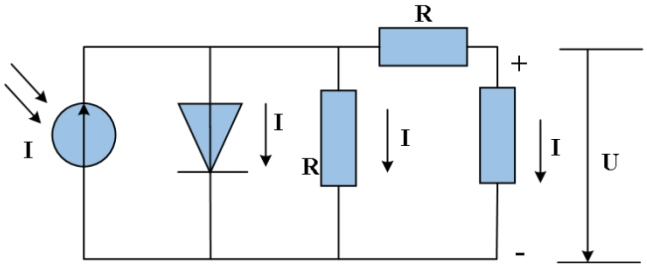

Figure 2. Equivalent circuit diagram of photovoltaic power generation

Solar irradiance and ambient temperature are the key determinants of the output power in a photovoltaic generation system. In actual operation, the photovoltaic array's output power is given as equation (1):

$$P_{pv}(t) = P_{stc} \cdot \frac{G(t)}{G_{stc}} \cdot [1 + k(T(t) - T_{stc})] \quad (1)$$

$P_{pv}(t)$ represents the actual output power of the photovoltaic array at time t. P_{stc} and G_{stc} are rated power measured and reference irradiance under a standard test condition (STC). Actual irradiance and ambient temperature at t are expressed as $G(t)$ and $T(t)$. The power temperature coefficient k reflects some extent to which temperature changes affect output power. T_{stc} refers to the standard test temperature.

Wind and solar energy exhibit a natural complementary distribution over time. In summer, when sunlight is abundant, photovoltaic power generation is high, while wind resources in most regions are relatively weak, limiting wind turbine output. The opposite is true in winter: wind power often increases when sunlight weakens. This natural complementarity provides optimization space for microgrid power source configuration. During the planning phase, a planning strategy that leverages the complementary characteristics of wind and solar energy through rational capacity allocation can effectively improve the system's overall power supply stability. At the same time, it can reduce reliance on energy storage equipment, thus achieving better economic benefits.

The relationship between wind turbine output power and wind speed is described using a piecewise function. Here, v is the actual wind speed at hub height; $P_{wt}(t)$ and P_r represent the wind turbine's actual output and rated power. v_{ci} denotes the cut-in wind speed at which the wind turbine starts generating power. v_r is the rated wind speed required to achieve the rated output power. v_{co} refers to the cut-out wind speed at which the wind turbine shuts down for safety reasons.

$$P_{wt}(t) = \begin{cases} 0 & v < v_{ci} \text{ or } v > v_{co} \\ P_r \cdot \frac{v - v_{ci}}{v_r - v_{ci}} & v_{ci} \le v < v_r \\ P_r & v_r \le v \le v_{co} \end{cases} \quad (2)$$

(2) Electrolyzer model

Electrolyzers produce hydrogen by consuming electrical energy, and their hydrogen production capacity depends on the input electrical power and operational efficiency. The efficiency of electrolyzers changes under partial load conditions, a characteristic that needs to be considered in the model:

$$m_{H_2,ele}(t) = \frac{\eta_{ele}(P_{ele}(t)) \cdot P_{ele}(t)}{LHV_{H_2}} \quad (3)$$

$m_{H_2,ele}(t)$ is the hydrogen production at time t. The electrical power input to the electrolyzer at time t is expressed by $P_{ele}(t)$. η_{ele} is the hydrogen production efficiency of the electrolyzer, which varies with changes in input power. LHV_{H_2} is hydrogen's lower heating value, i.e., the energy released by the complete combustion of unit mass.

(3) Hydrogen storage tank model

Hydrogen storage tanks store surplus hydrogen in the system, and their inventory status changes dynamically over time. The inventory of hydrogen storage tanks can be defined as:

$$E_{H_2}(t) = E_{H_2}(t-1) + m_{H_2,in}(t) - m_{H_2,out}(t) \quad (4)$$

The hydrogen inventory in the storage tank at the start of time t is represented by $E_{H_2}(t)$. $m_{H_2,in}(t)$ and $m_{H_2,out}(t)$ are the amount of hydrogen injected into and extracted from a storage tank during time t, respectively. Meanwhile, the inventory of the hydrogen storage tank must meet its design capacity constraints:

$$E_{H_2}^{min} \le E_{H_2}(t) \le E_{H_2}^{max} \quad (5)$$

(4) Fuel cell model

A fuel cell generates electricity by converting the chemical energy of hydrogen. The electrical power output is directly proportional to the hydrogen consumed mass flow rate.

$$P_{fc}(t) = \eta_{fc} \cdot m_{H_2,fc}(t) \cdot LHV_{H_2} \quad (6)$$

$P_{fc}(t)$ and $m_{H_2,fc}(t)$ denote the electrical power output and mass of hydrogen consumed by the fuel cell at time t. η_{fc} is the fuel cell's power generation efficiency. This study selects Proton Exchange Membrane Fuel Cells (PEMFC) as the technology solution in the microgrid system. Among various fuel cell technologies, PEMFC offers

advantages such as fast start-up speed, zero emissions during operation, and low operating temperature. Its working principle is revealed in Figure 3:

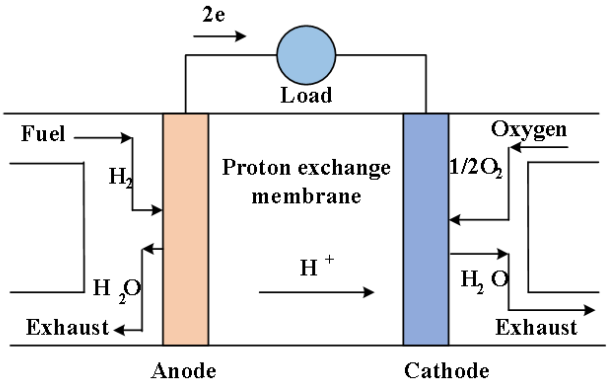

Figure 3. Schematic diagram of the working principle of PEMFC

(5) Grid interaction model

The microgrid exchanges electrical energy with the main grid through the PCC, and this exchange is limited by equipment capacity:

$$-P_{grid}^{max} \le P_{grid}(t) \le P_{grid}^{max} \quad (7)$$

$P_{grid}(t)$ is the power exchanged with the grid at time t; positive and negative values indicate purchasing and selling electricity to the grid. P_{grid}^{max} refers to the maximum allowable exchange power, determined by the capacity of the connecting equipment. The economic costs incurred by grid interaction need to be included in the total system operating cost. $c_{buy}(t)$ and $c_{sell}(t)$ are the electricity purchase and electricity sales prices at time t, respectively. Typically, the purchase price is higher than the sales price, and this price difference reflects the transmission and distribution costs and operating expenses of the grid. The total cost can be written as:

$$C_{grid}(t) = c_{buy}(t) \cdot \max\left(0, P_{grid}(t)\right) - c_{sell}(t) \cdot \min\left(0, P_{grid}(t)\right) \quad (8)$$

3.3. Multi-objective collaborative planning model

On the basis of completing the aforementioned system architecture design and mathematical model establishment, a multi-objective collaborative planning model is constructed for electro-hydrogen coupling microgrids. The model aims to simultaneously optimize the system's economic efficiency, environmental friendliness, and power supply reliability, providing a theoretical foundation for subsequent solution and decision analysis. The economic objective pursues the minimization of the present value of total system planning costs. This objective comprehensively considers factors such as initial equipment investment, operation and maintenance costs, grid electricity purchase costs, and electricity sales revenue. Through discounting, the cash flows throughout the full life cycle are uniformly converted to current value. Its mathematical expression is:

$$\min F_1 = C_{inv} + \sum_{t=1}^{T} \frac{C_{om}(t) + C_{grid,buy}(t) - R_{grid,sell}(t)}{(1+r)^t} \quad (9)$$

C_{inv} represents the initial equipment investment cost. $C_{om}(t)$, $R_{grid,sell}(t)$, and $C_{grid,buy}(t)$ denote the operation & maintenance cost, electricity sales revenue, and electricity purchase cost in year *t*. *r* refers to the discount rate, and *T* indicates the planning period. The environmental objective focuses on minimizing the system's total life-cycle carbon emissions. This objective mainly considers the indirect carbon emissions generated by purchasing electricity from the main grid, and quantifies the environmental impact of system operation by introducing grid carbon emission factors. $P_{grid,buy}(t,i)$ stands for the electricity purchase power in the i-th time of year t. $\varphi_{grid}(t)$ means the grid carbon emission factor in year t. Δt signifies the time length; N_t is the total number of time periods in a year.

$$\min F_2 = \sum_{t=1}^{T} \sum_{i=1}^{N_t} \left[P_{grid,buy}(t,i) \cdot \varphi_{grid}(t) \cdot \Delta t\right] \quad (10)$$

The power supply reliability objective adopts the reciprocal of the Expected Energy Not Supplied (EENS) as the evaluation index. It can effectively reflect the system's continuous power supply capacity, with a higher value indicating higher reliability:

$$\max F_3 = \frac{1}{EENS} = \frac{1}{\sum_{t=1}^{T} \sum_{i=1}^{N_t} \max\left(0, P_{load}(t,i) - P_{avail}(t,i)\right) \cdot \Delta t} \quad (11)$$

$P_{load}(t,i)$ represents the load demand in the i-th time of year t. $P_{avail}(t,i)$ stands for the system's total available power generation in that period.

Model solution needs to satisfy the system's physical laws and engineering operation requirements. These constraints collectively ensure that the planning scheme can operate safely. Among them, electrical power balance is the foundation for stable system operation. This constraint ensures that power generation and power consumption are balanced at any time. The left side of the equation includes photovoltaic output $P_{pv}(t)$, fuel cell power generation $P_{fc}(t)$, wind turbine output $P_{wt}(t)$, and grid interaction power $P_{grid}(t)$. The right side corresponds to electrical load $P_{load}(t)$, electrolyzer power consumption $P_{ele}(t)$, and curtailment power of wind-solar energy $P_{curt}(t)$.

$$P_{pv}(t) + P_{wt}(t) + P_{fc}(t) + P_{grid}(t) = P_{load}(t) + P_{ele}(t) + P_{curt}(t) \quad (12)$$

The hydrogen system balance constraint ensures the coordinated relationship between hydrogen production, consumption, and storage:

$$m_{H_2,ele}(t) + m_{H_2,buy}(t) = m_{H_2,fc}(t) + m_{H_2,load}(t) + \left[E_{H_2}(t) - E_{H_2}(t-1)\right] \quad (13)$$

Hydrogen sources include electrolyzer hydrogen production $m_{H_2,ele}(t)$, ele}(t)\) and purchased hydrogen $m_{H_2,buy}(t)$; they are used to meet fuel cell hydrogen consumption $m_{H_2,fc}(t)$ hydrogen load demand $m_{H_2,load}(t)$, and possible changes in hydrogen storage tank inventory. Equipment operation constraints ensure that each component operates under safe conditions:

$$P_i^{min} \le P_i(t) \le P_i^{max} \quad (14)$$

$$|P_i(t) - P_i(t-1)| \le \Delta P_i^{max} \quad (15)$$

These constraints ensure that the equipment output $P_i(t)$) always remains within the technically allowed range, and the power change rate does not exceed the maximum ramping capacity ΔP_i^{max}. In addition, the operation of hydrogen storage tanks also needs to meet capacity constraints. This constraint ensures that the hydrogen storage tank inventory $E_{H_2}(t)$ is always maintained within a safe range, avoiding overcharging risks and ensuring necessary emergency reserves. The grid interaction power is constrained by the connection point equipment's capacity. It ensures that the power exchange $P_{grid}(t)$ between the microgrid and the main grid does not exceed the maximum allowable value P_{grid}^{max}, ensuring the safety of grid-connected operation.

$$-P_{grid}^{max} \le P_{grid}(t) \le P_{grid}^{max} \quad (16)$$

This study also uses binary variables to characterize equipment selection and installation decisions to constrain topological logic. Among them, $x_i = 1$ indicates the selection and installation of equipment i; $x_i = 0$ is non-installation. This constraint realizes the mathematical description of discrete decision variables.

$$x_i \in \{0,1\} \quad (17)$$

The system reliability constraint ensures that the system's EENS does not exceed the maximum allowable value $EENS^{max}$, thereby guaranteeing the reliability of the user's power supply.

$$EENS \le EENS^{max} \quad (18)$$

3.4. Design of a multi-objective solution algorithm

To address the electro-hydrogen coupling microgrid planning's complex optimization problems, this study adopts NSGA-II with an elitist strategy for solutions. This algorithm performs excellently in handling MOO problems; it is particularly suitable for solving the established mixed-integer nonlinear programming model, which includes both continuous and discrete variables. The electro-hydrogen coupling microgrid planning problem is high-dimensional and nonlinear, and NSGA-II has remarkable advantages in handling such complex problems. The algorithm adopts a fast non-dominated sorting mechanism, which can effectively identify optimal solutions at different levels, ensuring the convergence of solutions. Meanwhile, by introducing a crowding distance comparison operator, the algorithm can obtain a uniformly distributed set of Pareto optimal solutions in the objective space, providing decision-makers with diverse options.

To convert the grid planning problem into a chromosome form more easily handled by genetic algorithms, this study designs an encoding structure as presented in Figure 4. The chromosome adopts a hybrid encoding method, including equipment siting, capacity, and operation strategy encodings. For equipment siting, binary encoding is used to represent the equipment installation status at each candidate node. For example, for wind turbine installation locations, a binary string of length N is used, where each bit represents a candidate node; a value of 1 indicates the installation of a wind turbine at that node, and 0 represents no installation. Real-number encoding is then used to represent the installation capacity of each equipment. For equipment determined to be installed in the siting encoding, its capacity takes continuous values within preset upper and lower limits. The operation strategy encoding uses real-number encoding to represent typical daily operation schemes; these cover the operating power of electrolyzers and fuel cells at each time period, as well as the exchange power with the grid.

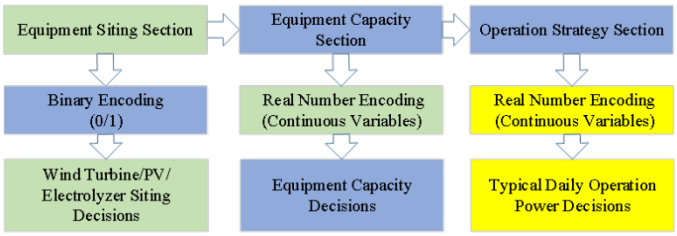

Figure 4. The working principle of PEMFC

The NSGA-II algorithm's solution process is plotted in Figure 5. First, an initial population of size N is randomly generated, with each individual representing a complete planning scheme containing detailed information such as siting, capacity, and operation strategy. The chromosome is then decoded into a specific planning scheme, which is input into the system simulation model to calculate the operation of each scheme throughout the full life cycle. Based on the simulation results, the three objective function values of each scheme are calculated. For individuals violating constraints, a penalty function method is adopted to reduce their fitness. Next, fast non-dominated sorting is performed on the individuals in the population. This process divides individuals into different non-dominated levels. Within the same level, the crowding distance quantifies the distribution density of each solution individual in the objective space.

During selection, crossover, and mutation, a binary tournament selection operator is adopted, giving priority to individuals with high non-dominated levels and large crowding distances. Simulated binary crossover and polynomial mutation are carried out on the selected individuals to generate offspring populations. Finally, the parent and offspring populations are merged, and non-dominated sorting and crowding distance calculation are performed again. The top N optimal individuals are selected to form a new parent population. The above steps are repeated until the convergence condition is met, and the iteration stops. A uniformly distributed set of Pareto optimal solutions is finally output. Thus, it offers decision-makers multiple grid configuration planning schemes that balance economic efficiency, environmental friendliness, and reliability.

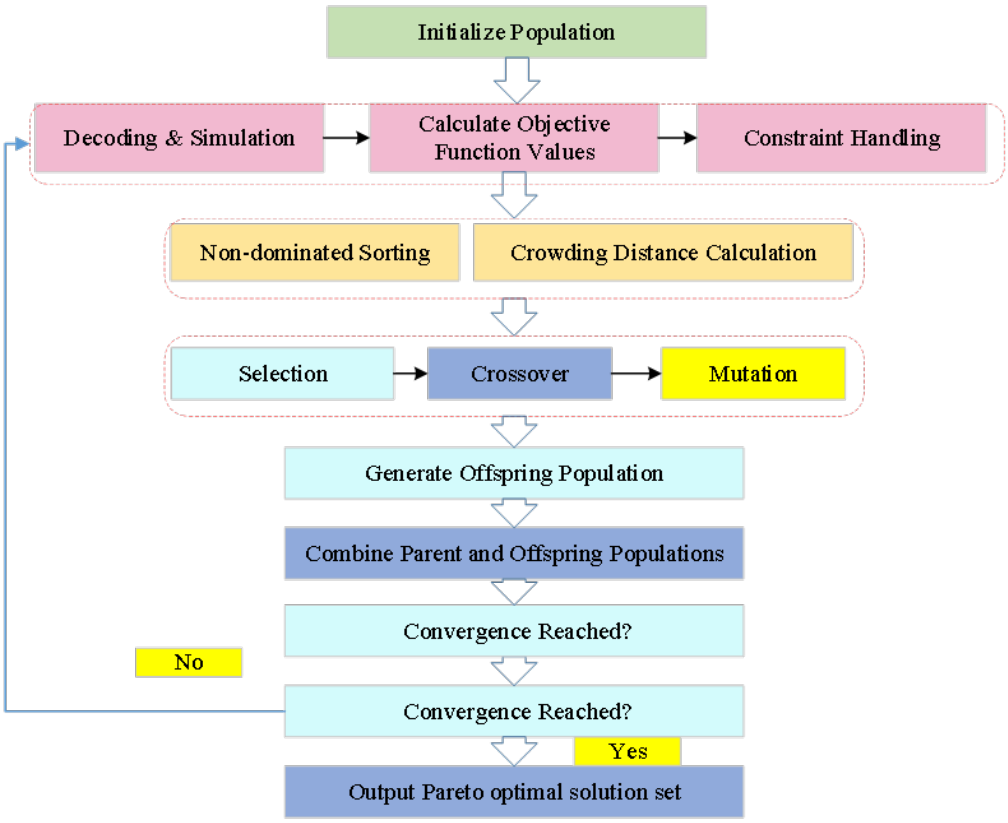

Figure 5. The solution process of the NSGA-II algorithm

3.5. Case background and data sources

To verify the proposed planning model and algorithm's effectiveness, this section selects actual data from a coastal industrial park in eastern China as a research case for simulation analysis. The park is endowed with abundant wind and solar resources and has a clear hydrogen energy demand. The annual average irradiance is 1580 (kilowatt-hour per square meter) kWh/m², the annual average wind speed and electrical load is 6.8 meters per second (m/s) and 685 kW; the AC/DC load ratio is approximately 2:1; and the daily average hydrogen load demand is about 50 kilograms (kg). Table 1 lists the cost parameters of the main system equipment. These data are derived from recent market research and supplier quotes, reflecting the technical and economic characteristics of current mainstream equipment. Table 2 shows the TOU electricity pricing scheme applicable to the park, which divides a day into three periods, each corresponding to different purchase and sales prices.

Table 1. Technical cost parameters of key equipment

	Capacity unit	Investment cost (Yuan/unit)	Service life (years)	Operation and maintenance rate
Photovoltaic systems	kW	8,200	25	3%
Wind turbines	kW	11,500	20	3%
Lithium-ion batteries	kWh	1,200	15	2%
Proton exchange membrane electrolyzers	kW	18,500	15	4%
Fuel cells	kW	13,500	15	4%
High-pressure hydrogen storage tanks	kg	2,200	20	2%

Table 2. TOU electricity pricing scheme for the park

Time period division	Time range	Purchase price (Yuan/kWh)	Sale price (Yuan/kWh)
Off-peak period	00:00-08:00	0.35	0.25
Peak period	08:00-12:00 17:00-21:00	0.85	0.68
Rush hour period	12:00-17:00 21:00-24:00	0.65	0.50

4. Results and Discussion

4.1. Analysis of MOO results

Through a solution with the NSGA-II algorithm, this study obtains the set of Pareto optimal solutions for the electro-hydrogen coupling microgrid planning problem. These solutions form a clear surface in the three-dimensional objective space, revealing the complex trade-off relationships between different optimization objectives. From the distribution characteristics of the solution set, there are remarkable competitive relationships between the three objectives. The economic objective and the environmental objective exhibit a strong negative correlation—reducing system carbon emissions usually requires increasing investment costs. This relationship is manifested as an obvious transition zone in the solution space. To more intuitively demonstrate the differences in system configuration under diverse optimization objectives, this study selects three typical schemes for detailed analysis. Figure 6 demonstrates the key performance indicators of these three schemes. Scheme A prioritizes economic efficiency, with the lowest investment cost but poor performance in environmental friendliness and reliability. Scheme C achieves near-zero carbon emissions and high reliability, but its total investment cost is 42% higher than that of Scheme A. Scheme B keeps a good balance between the three objectives, exchanging a 28% increase in cost for a 54% reduction in carbon emissions and a 55% improvement in reliability, displaying the best comprehensive benefits.

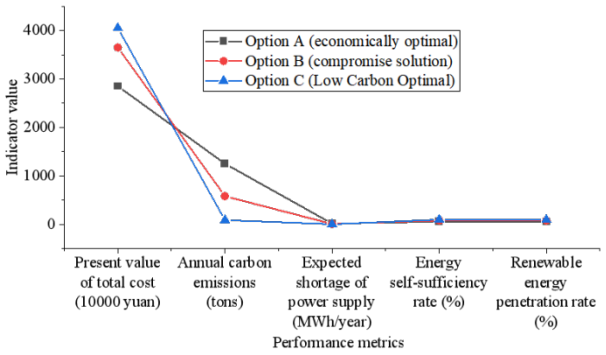

Figure 6. Performance comparison of typical planning schemes

The differences in equipment configuration among these schemes further confirm the trade-off relationships between objectives. Figure 7 illustrates the key equipment capacity configuration of each scheme. It can be found that as the optimization objective shifts from economic efficiency to environmental friendliness, the configuration scale of renewable energy and hydrogen energy systems increases significantly. Through in-depth analysis of the Pareto solution set, this study identifies an evident "cost inflection point" region. Within this region, the marginal benefit of the scheme is the highest. In other words, each additional unit of investment yields the greatest improvement in environmental friendliness and reliability.

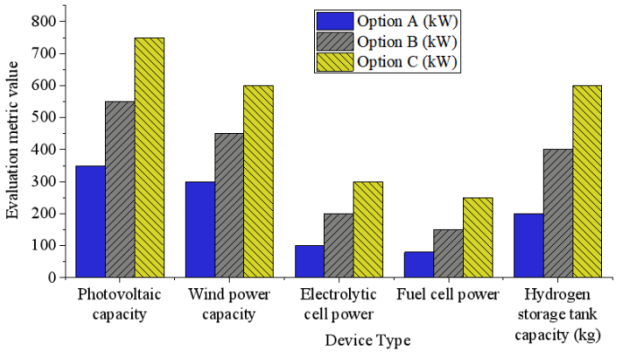

Figure 7. Equipment configuration comparison in typical schemes

Through annual 8760-hour time-series simulation, this study obtains the typical operational characteristics of each scheme. Figure 8 shows the power balance of each scheme on a typical day. Scheme A has a relatively small installed capacity of renewable energy, and its power supply relies heavily on the external grid. As a result, the electrolyzer's operating time is limited. To optimize operational economic efficiency, the fuel cell's start-stop strategy is obviously guided by peak-valley electricity prices; it mainly chooses to operate during peak electricity price periods to reduce the system's overall electricity cost. However, Scheme B has good self-balancing capacity, with

the curtailment rate of renewable energy controlled within 5%, indicating that the hydrogen energy system plays an important regulatory role. Scheme C achieves almost complete self-sufficiency, with minimal exchange power with the grid. Besides, the hydrogen energy system undertakes the important roles of cross-seasonal energy storage and power balance.

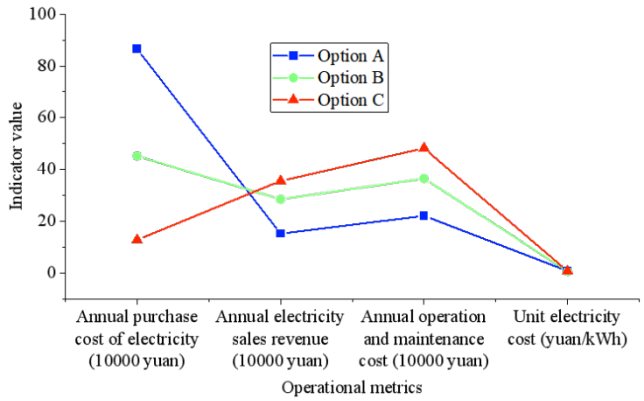

Figure 8. Comparison of annual operational economic indicators of different typical scheme

4.2. Sensitive analysis

The decline in equipment costs, especially the cost of hydrogen energy systems, is a significant trend in current energy technology development. In contrast, carbon pricing policies are important market mechanisms driving energy transition. In Figure 9, when the electrolyzer investment cost decreases by 30%, the optimal system configuration undergoes prominent changes. The electrolyzer installation capacity rises from 150 kW in the baseline scenario to 220 kW, an increase of 46.7%. This change directly drives the coordinated growth of renewable energy capacity, with photovoltaic and wind power capacities increasing by 8.6% and 4.0%, respectively. This indicates that cost reduction makes hydrogen production using surplus renewable energy more economically attractive, and the system's ability to absorb renewable energy through the "electricity-hydrogen" conversion path is enhanced. When the total system cost drops by 6.3%, annual carbon emissions decrease by 10.3%, reflecting the dual promoting effect of declining hydrogen energy costs on system economic efficiency and environmental friendliness. When the fuel cell cost decreases by 25%, its installation capacity increases by 29.2% accordingly. This enhances the system's power supply guarantee capacity when renewable energy output is insufficient; this enables the system to more boldly configure renewable energy, thereby further reducing carbon emissions.

In contrast, the impact of a 20% decrease in photovoltaic costs is more far-reaching. This change directly triggers the restructuring of the system's power source structure: photovoltaic capacity increases greatly by 37.1%, while wind power capacity decreases by 12.0% accordingly. This "trade-off" relationship reflects the wind and solar output's complementary characteristics and the resources' competitive relationship in the optimization model. The remarkable advantage of photovoltaic costs makes it account for a larger proportion of power sources; it also drives a 13.3% increase in electrolyzer capacity to absorb more surplus photovoltaic power.

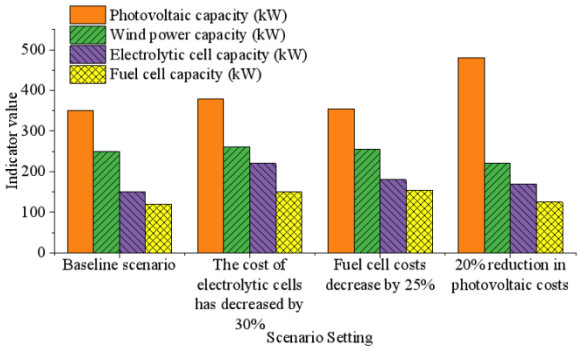

(a)

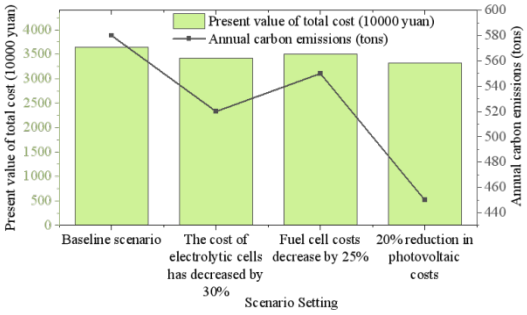

(b)

Figure 9. The impact of equipment cost changes on optimal configuration. (a) System capacity configuration; (b) Cost and carbon emissions

At the policy level, Figure 10 reveals that as the carbon price gradually increases from zero to 300 yuan/ton, the total cost of Scheme A rises markedly by 29% due to carbon cost expenditures, and its economic advantage weakens accordingly. When the carbon price exceeds 200 yuan/ton, the cost advantage of the compromise Scheme B begins to emerge, with its growth rate noticeably lower than that of Scheme A. This transition has important policy implications. It indicates that reasonable carbon pricing can effectively bridge the cost gap between traditional economic schemes and low-carbon schemes, providing economic incentives for low-carbon transition. Meanwhile, the cost of the scheme grows most gently with the increase in carbon price, showing its resilience in coping with the risk of rising carbon costs.

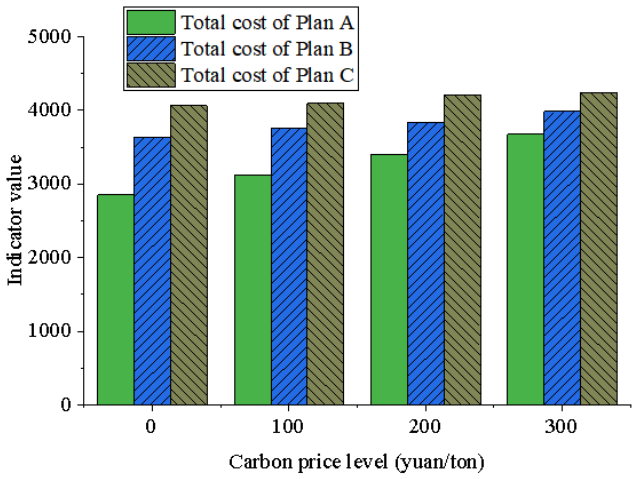

Figure 10. The impact of carbon pricing policy on the total cost of each plan (in ten thousand yuan)

4.3. Discussion

The above results underscore that compared with traditional single-objective planning, the MOO method adopted here can provide more comprehensive decision support. It demonstrates system configuration schemes under different objective orientations. The research results verify the ability of the electro-hydrogen coupling system to improve renewable energy absorption capacity and ensure power supply reliability; it is consistent with the research conclusions of Egeland-Eriksen et al. [16]. From a technical and economic perspective, the "cost inflection point" phenomenon discovered in this study has important engineering significance. Before the inflection point, moderate investment increases can significantly improve system environmental friendliness and reliability; this echoes the research results of Blackhurst et al. [17] on the marginal benefits of energy systems. However, after exceeding the inflection point, the marginal benefit of investment drops sharply. This is similar to the "over-investment" phenomenon reported by Bin & Sun [18]. Therefore, in practical engineering applications, decision-makers should focus on planning schemes near the inflection point to maximize investment benefits. The optimization results of this study can provide reference for microgrid planning in similar regions [19]. Especially for coastal industrial parks with abundant wind and solar resources and hydrogen energy demand, the electro-hydrogen coupling technology route has distinct advantages. However, in practical applications, specific factors such as local grid conditions, load characteristics, and policy environments need to be considered to appropriately adjust the planning scheme.

5. Conclusion

This study explores the collaborative planning problem of microgrid electro-hydrogen coupling systems. It establishes a new planning framework that considers both topological structure and dynamic development dimensions while balancing multiple optimization objectives. The study finds that electro-hydrogen coupling technology can substantially improve the comprehensive performance of microgrids. Through the introduction of hydrogen energy systems, large-scale absorption and cross-time storage of renewable energy are successfully achieved, and power supply reliability is significantly enhanced. This furnishes key technical support for addressing the volatility problem caused by high-proportion renewable energy integration. The study also discovers an important phenomenon—the multi-objective "cost inflection point". This phenomenon indicates that optimal planning does not pursue the extremum of a single indicator but rather finds a balance between economic efficiency, environmental friendliness, and reliability. Before the inflection point, appropriate additional investment can significantly improve system performance; after outperforming the inflection point, the benefit of continued investment decreases significantly. This finding provides an important reference for engineering investment decisions. However, this study conducts optimization based on deterministic scenario data and fails to fully consider the randomness of wind and solar output and the uncertainty of load forecasting. This may affect the adaptability of the planning scheme in actual operation. In addition, the model mainly focuses on optimization at the technical and economic levels, with relatively limited consideration of external factors such as power market environments and policy changes. Future plans include introducing stochastic programming or robust optimization methods to explicitly consider the uncertainty of renewable energy output and load demand, enhancing the planning schemes' robustness. Further research can also incorporate external environmental factors, such as power market mechanisms and carbon trading policies, into the model to analyze the system evolution law under the coupling effect of multiple factors.

References

[1] Islam M M, Yu T, Giannoccaro G, et al. Improving reliability and stability of the power systems: A comprehensive review on the role of energy storage systems to enhance flexibility[J]. IEEE Access, 2024, 12: 152738-152765.

[2] Meng Q, Tong X, Hussain S, et al. Enhancing distribution system stability and efficiency through multi-power supply startup optimization for new energy integration[J]. IET Generation, Transmission & Distribution, 2024, 18(21): 3487-3500.

[3] Yang B, Tao J, Yin X, et al. Large-signal stability analysis and enhancement strategy of ITER power supply system[J]. International Journal of Electrical Power & Energy Systems, 2025, 172: 111217.

[4] Banihabib R, Fadnes F S, Assadi M. Techno-economic optimization of microgrid operation with integration of renewable energy, hydrogen storage, and micro gas turbine[J]. Renewable Energy, 2024, 237: 121708.
[5] Zhang C, Rezgui Y, Luo Z, et al. Simultaneous community energy supply-demand optimization by microgrid operation scheduling optimization and occupant-oriented flexible energy-use regulation[J]. Applied Energy, 2024, 373: 123922.
[6] Ahsan S M, Musilek P. Optimizing Multi-Microgrid Operations with Battery Energy Storage and Electric Vehicle Integration: A Comparative Analysis of Strategies[J]. Batteries, 2025, 11(4): 129.
[7] Goyal A, Bhattacharya K. Optimal design of a decarbonized sector-coupled microgrid: electricity-heat-hydrogen-transport sectors[J]. IEEE Access, 2024, 12: 38399-38409.
[8] Shi T, Zhou H, Shi T, et al. Research on energy management in hydrogen–electric coupled microgrids based on deep reinforcement learning[J]. Electronics, 2024, 13(17): 3389.
[9] Balu V, Krishnaveni K, Malla P, et al. Improving the power quality and hydrogen production from renewable energy sources based microgrid[J]. Engineering Research Express, 2023, 5(3): 035037.
[10] Alsalloum H, Merghem-Boulahia L, Rahim R. A systematical analysis on the dynamic pricing strategies and optimization methods for energy trading in smart grids[J]. International Transactions on Electrical Energy Systems, 2020, 30(9): e12404.
[11] Temiz M, Dincer I. Development and assessment of an onshore wind and concentrated solar based power, heat, cooling and hydrogen energy system for remote communities[J]. Journal of Cleaner Production, 2022, 374: 134067.
[12] Moritz M, Schönfisch M, Schulte S. Estimating global production and supply costs for green hydrogen and hydrogen-based green energy commodities[J]. International Journal of Hydrogen Energy, 2023, 48(25): 9139-9154.
[13] Quan S, Wang Y X, Xiao X, et al. Real-time energy management for fuel cell electric vehicle using speed prediction-based model predictive control considering performance degradation[J]. Applied Energy, 2021, 304: 117845.
[14] Teo T T, Logenthiran T, Woo W L, et al. Optimization of fuzzy energy-management system for grid-connected microgrid using NSGA-II[J]. IEEE transactions on cybernetics, 2020, 51(11): 5375-5386.
[15] Su R, He G, Su S, et al. Optimal placement and capacity sizing of energy storage systems via NSGA-II in active distribution network[J]. Frontiers in Energy Research, 2023, 10: 1073194.
[16] Egeland-Eriksen T, Hajizadeh A, Sartori S. Hydrogen-based systems for integration of renewable energy in power systems: Achievements and perspectives[J]. International journal of hydrogen energy, 2021, 46(63): 31963-31983.
[17] Blackhurst M, Venkatesh A, Sinha A, et al. Marginal abatement costs for greenhouse gas emissions in the United States using an energy systems approach[J]. Environmental Research: Energy, 2025, 2(1): 015012.
[18] Bin S, Sun G. Research on the influence maximization problem in social networks based on the multi-functional complex networks model[J]. Journal of Organizational and End User Computing (JOEUC), 2022, 34(3): 1-17.
[19] Russo C, Cirillo V, Pollaro N, et al. The global energy challenge: second-generation feedstocks on marginal lands for a sustainable biofuel production[J]. Chemical and Biological Technologies in Agriculture, 2025, 12(1): 10.